Available online at www.sciencedirect.com
SCIENCE DIRECT®
Continental Shelf Research 25 (2005) 1692–1711
CONTINENTAL SHELF RESEARCH
www.elsevier.com/locate/csr

Satellite ocean color observations of stormwater runoff plumes along the San Pedro Shelf (southern California) during 1997–2003

Nikolay P. Nezlin[a,*], Paul M. DiGiacomo[b]

[a]*Southern California Coastal Water Research Project, 7171 Fenwick Lane, Westminster, CA 92683, USA*
[b]*Jet Propulsion Laboratory, California Institute of Technology, Pasadena, CA 91109, USA*

Received 24 June 2004; received in revised form 24 February 2005; accepted 11 May 2005
Available online 15 July 2005

Abstract

Knowledge of freshwater runoff plume dynamics in southern California is important for management of coastal water quality, because river discharge associated with episodic winter rainstorms can be a major source of pollutants and pathogens to coastal waters. The purpose of this study was to analyze the spatio-temporal dynamics of plumes at the San Pedro Shelf in southern California and identify factors influencing the incidence and dispersal patterns of plumes. We used 1.1-km spatial resolution satellite images collected in 1997–2003 by the SeaWiFS optical radiometer. The area of each plume was detected by the backscattering characteristics of surface waters in the vicinity of the mouths of four rivers that discharge to the San Pedro Basin. The rainstorm magnitude was estimated from atmospheric precipitation averaged over the total area of local watersheds. The plume size estimated from the backscattering coefficient $nLw555 > 1.3\,mW\,cm^{-2}\,\mu m^{-1}\,sr^{-1}$ was highly correlated with the amount of rainwater precipitated over the watershed area and accumulated during the period preceding the plume. The relation between rainstorm and plume area was linear with zero intercept: that means that the minimum rainstorm magnitude under which no plume occurred in the study area was almost zero, and even small precipitation resulted in a plume. The persistence of the plumes was estimated by fitting the coefficients of the model of plume water dissipation to achieve maximum correlation between the plume area and rainstorm: Twenty-five percent of rainwater dissipated daily, which gradually decreased the plume size. The size, alongshore and cross-shelf translocation of the plumes were modulated slightly by the local circulation, forced remotely by the equatorward wind a few hundred km to the south (along the coast of Baja California). The influence of tidal circulation on the plume area was slight and statistically insignificant.

Keywords: Ocean color; Freshwater discharge; Plumes; Precipitation; San pedro shelf; 33.47–33.79°N; 118.4–117.7 W

*Corresponding author. Tel.: +1 714 372 9227; fax: +1 714 894 9699.
E-mail address: nikolayn@sccwrp.org (N.P. Nezlin).

0278-4343/$ - see front matter © 2005 Elsevier Ltd. All rights reserved.
doi:10.1016/j.csr.2005.05.001

1. Introduction

Southern California is characterized by a series of well-developed, steep watersheds that are subject to extremely dynamic episodic runoff events, primarily resulting from large winter rainstorms. These runoff events result in an increase of pollutants and pathogens in near-shore waters, which can adversely affect coastal ocean and beach water quality (Ackerman and Weisberg, 2003; Bay et al., 2003; Schiff and Bay, 2003). The knowledge of storm water plume dynamics (i.e., size, duration and persistence, propagation speed and direction) can help coastal managers make more informed decisions about managing beach water quality following storms.

Our knowledge of plume dynamics to date is primarily based on data collected by traditional oceanographic methods, i.e., using instruments onboard coastal research vessels. These field measurements can provide accurate assessments of multiple water quality parameters at the ocean surface and at depth. However, it is difficult to estimate pollutant dispersal patterns solely from field measurements. Field measurements typically are restricted, due to sampling logistics, cost, weather, or other issues, to a limited number of stations (and/or samples) that are usually inadequate to resolve and characterize plume dynamics in both space and time.

Another option for studying stormwater runoff plume dynamics is satellite imagery. Satellite images can provide synoptic and frequent regional overviews that enable more effective analysis of the spatial and temporal distribution of these plumes via surface parameters that can be measured from space. In field studies, runoff plumes are best characterized by their signature of decreased salinity. Unfortunately, salinity is not presently measured from space and planned sensors will not have adequate spatial resolution to resolve the types of plumes under consideration here (Lagerloef, 2000). However, satellites can observe other characteristics of coastal surface waters that are impacted by the plume, such as sea-surface roughness as measured by Synthetic Aperture Radar (SAR) (e.g., Svejkovsky and Jones, 2001; DiGiacomo et al., 2004) or sea spectral reflectance as measured by "ocean color" images. Indeed, satellite ocean color observations of the optical properties of coastal surface waters can be used to distinguish plume water from ambient water masses, particularly based on increased concentrations of suspended material in the plumes (Mertes et al., 1998; Sathyendranath, 2000; Mertes and Warrick, 2001). The correlation between the optical properties of surface waters and salinity has been demonstrated in many ocean regions (Monahan and Pybus, 1978; Vasilkov et al., 1999; Siddorn et al., 2001). As such, the optical signatures of river plumes can be used as a proxy for salinity to study their spatio-temporal distribution. In this study, we perform synoptic time-series analyses of the correlation between freshwater runoff plumes and rainstorms by leveraging frequent and ongoing satellite ocean color observations. Cloud cover leading to missing data is a common occurrence in ocean color imagery. However, in southern California the high-pressure systems following winter storms typically clear the skies and help mitigate this effect. The daily acquisition of ocean color data also helps to overcome this constraint.

In this article, we perform the first regional study to evaluate the role of different meteorological and oceanographic factors on plume dynamics, based on more than 6 years of satellite observations of ocean color. Presently, the quantitative relationship between plume size and persistence, and meteorological and hydrological conditions (primarily rainstorm magnitude) is poorly understood. We have no estimates of what part of the precipitated water forms the plume and what part is retained in the watershed. Further, the dispersal patterns of pollutants and pathogens discharged to the coastal ocean, largely regulated by stormwater plume dynamics, are unclear and require further analysis. The behavior of small river plumes depends on the local near-shore circulation, which is poorly understood in the study area. The role of tides in plume dispersion is also poorly known: the influence of the range of tidal variability on plume behavior depends on local bottom topography and is different in each coastal region. To some extent, we might expect that an intensive local circulation during spring

tides would result in an increase of plume size due to more intensive onshore/offshore circulation. However, more intensive tidal movements can also erode the plume and decrease its size.

Within this context, stormwater runoff plume areas along a heavily impacted section of the southern California coast (i.e., the San Pedro Shelf) were estimated from daily 1.1-km resolution Sea-viewing Wide Field-of-view Sensor (i.e., SeaWiFS) ocean color satellite imagery. Normalized water-leaving radiation was used in the green-yellow spectral region, i.e., at the 555 nm wavelength (nLw555), which is most sensitive to the concentration of suspended sediments in the upper ocean layer (Lira et al., 1997; Lahet et al., 2001; Loisel et al., 2001; Toole and Siegel, 2001). In this study, the basic concept is that a plume is the result of a rainstorm; so, the parameters of analysis (nLw555 value indicating the plume and the methods of data transformation) should be optimized to achieve maximum correlation between plume area and rainstorm magnitude. Other water column processes and constituents contributing to the color of surface waters (e.g. sediment resuspension in the shallow coastal zone, phytoplankton and biogenous material concentrations) are treated as noise in the relationship between the "signals" (rainstorms, wind, and tidal forcing) and the "response" (plume characteristics).

Our goals are:

- to identify the value of normalized water-leaving radiance (nLw555), which best characterizes the boundaries of the San Pedro Shelf runoff plume zone;
- to quantify the areas of the plumes observed by SeaWiFS radiometer from the beginning of the SeaWiFS mission (fall 1997) to June 2003;
- to find maximum correlation between the plume area and the amount of water discharged from the coastal watersheds;
- to evaluate the persistence of the river plumes (i.e., how long the signal of freshwater discharge is retained by the nearshore coastal ocean); and
- to analyze the influence of the local circulation forced by tides and local and remote wind on the size and alongshore translocation of these plumes.

2. San Pedro Shelf area and adjacent watersheds

The river flow in the four main watersheds discharging freshwater to the coastal zone of the San Pedro Basin (the Dominguez Channel, the Los Angeles River, the San Gabriel River, and the Santa Ana River; see Fig. 1) off the southern California coast is regulated by land cover, groundwater replenishment, and a number of flood control dams. An unknown quantity of rainwater is retained within flood control reservoirs (Turhollow, 1975; Gumprecht, 1999). Flood events resulting from rainstorms contribute more than 95% of the total runoff volume (Schiff et al., 2000). However, the contribution of non-storm-related flows to freshwater discharge and, in turn, to plume formation is unknown; it may be significant during the dry season (Ackerman et al., 2005). In particular, at this time a substantial amount of water (more than $680 \times 10^6\,m^3\,year^{-1}$) is imported by the Metropolitan Water District of Southern California from northern California and the Colorado River (MWD, 2002) and an unknown portion of this water can be diverted into river runoff and reach the ocean.

Three of four major rivers flowing to the San Pedro Basin discharge into the Los Angeles/Long Beach harbor complex, which can lead to concentration and retention of pollutants due to reduced exchange with offshore waters (DiGiacomo et al., 2004). Outside the harbor, near-shore

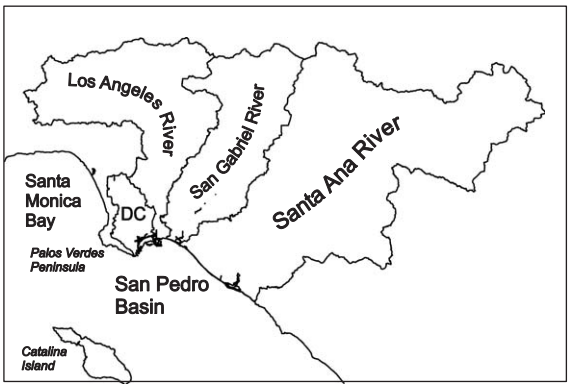

Fig. 1. San Pedro Shelf System: Map of watersheds of the Dominguez Channel (DC), Los Angeles River, San Gabriel River, and Santa Ana River and the adjacent coastal zone.

current patterns in the San Pedro Basin are complex and variable (Hickey, 1992; DiGiacomo and Holt, 2001). They are regulated by bottom topography as well as local and remote wind forcing. The San Pedro shelf is wider than elsewhere along the southern California coast (Fig. 2). This width influences coastal circulation and, in turn, the pattern of dispersion of freshwater discharged to that area. River discharge to this shallow shelf zone increases the concentration and retention of pollutants and can exacerbate its hazardous impacts, compared to regions with narrow shelves located to the north and to the south. The San Pedro Basin is a part of the Southern California Bight, separated from the west by the San Pedro Channel and from the southwest by Catalina Island. Circulation in the Southern California Bight is determined by an unsteady complex pattern of surface currents (Lynn and Simpson, 1987; Hickey, 1992, 1993). The waters of the southward-flowing California Current penetrate from the northwest, this flow being especially intensive in spring (Dorman and Palmer, 1981; Hickey, 1993; Bray et al., 1999). The waters of the poleward Southern California Countercurrent (Sverdrup and Fleming, 1941) penetrate to the basin alongshore from the southeast. Poleward flow exhibits significant seasonal variations. Maximum poleward flow occurs in summer or early fall, and is also strong in winter; minimum equatorward flow occurs during spring (Hickey, 1979, 1993). In the narrow inshore shelf zone of southern California, the seasonal mean flow is equatorward (Winant and Bratkovich, 1981; Hickey, 1992); however, this flow is not steady but results from complex circulation processes including eddies, internal waves, tidal movements, and local wind forcing (e.g., DiGiacomo and Holt, 2001; DiGiacomo et al., 2002). Further, some of the hydrodynamical processes in

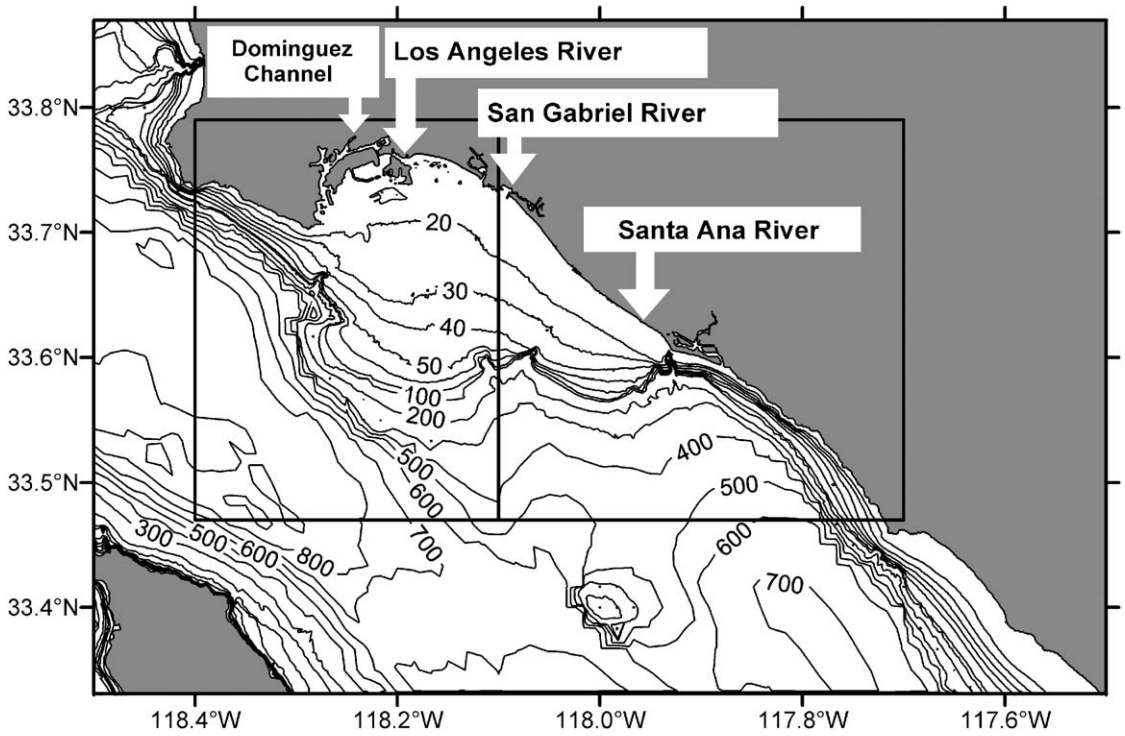

Fig. 2. Bottom topography of the San Pedro Shelf and the locations of the outlets of the four main watersheds (Dominguez Channel, Los Angeles River, San Gabriel River, and Santa Ana River). The rectangle indicates the area where nLw555 was averaged; the vertical line at 118.1°W was used for estimation of the plume position.

the Southern California Bight are remotely forced by wind stress a few hundred kilometers to the south at the coast of Baja California (Hickey et al., 2003; Pringle and Riser, 2003; Boehm et al., 2004).

3. Methods

In this study a river plume is defined as a water mass with a spectral reflectance (~color) different from that of the ambient water masses; this was assessed here using the values of normalized water-leaving radiation at a wavelength of 555 nm (nLw555). Plumes were identified using SeaWiFS radiometer data collected between October 6 (Julian Day 279) 1997 and June 26 (Julian Day 177) 2003. The high-resolution (1.1-km) optical measurements (Level 1A data) of the SeaWiFS radiometer (Acker et al., 2002) were obtained from the NASA Goddard Space Flight Center Distributed Active Archive Center (GSFC DAAC) and processed using SeaDAS software (Version 4.3). To calculate nLw555 normalized water-leaving radiances (Level 2 data), near-coincident NCEP meteorological and EPTOMS and TOVS ozone data files were obtained from GSFC DAAC and applied to corresponding SeaWiFS Level 1A data.

Accurate quantitative estimation of normalized water-leaving radiances (e.g., nLw555) in the near-shore region is frequently difficult because atmospheric correction algorithms can fail there. Further, one of the methodological questions here was whether to apply the mask removing the "stray light" effect. When this mask is applied, the nLw555 values of pixels located in the vicinity of areas with optical properties very different from ocean surface (e.g., land and clouds) are removed and as such near-shore structures (i.e., small plumes) are not resolved. Otherwise, these pixels obtain non-realistic overestimated values, which can be often treated as plumes. As a result, we decided to apply the "stray light" mask to all processed images and fill the gap between the land and water with interpolated nLw555 values. For this, the pixels of each resulting image of nLw555 were interpolated on the regular grid of $0.01^\circ \times 0.01^\circ$ (~1 km) spatial resolution. Missing data (MD) values were applied to the grid nodes located >2 km from the nearest "non-missing" pixel. The resulting images were analyzed visually to select the grids where the clouds did not cover the coastal zone and the pattern of freshwater plume (i.e., the zone of increased backscattering of sea surface) was visible. To quantitatively estimate the plume area, we filled the ocean zones containing MD (i.e., covered by the clouds) with interpolated nLw555 values. The grid nodes containing MD and located near the nodes with "non-missing" data were replaced with the interpolated nLw555 values obtained by averaging the surrounding grid nodes. Each step of this operation added "non-missing" data at the edge between the "non-missing" and MD (covered by clouds) areas. This operation was repeated until all grid nodes in the ocean zone were filled with "non-missing" data. The land mask was applied to the grid to remove (change to MD) the data unintentionally interpolated over the land. Each resulting image was compared visually to the image where the MD nodes were not filled with interpolated data to determine whether the "filling the gaps" procedure substantially distorted the plume pattern; if it did, the image was removed from the analysis.

The total number of analyzed SeaWiFS images was 628, collected from October 1997 to June 2003. This number indicates that useful satellite images were obtained on average every third day; during the remaining days, no SeaWiFS observations were obtained due to cloudy weather or acute satellite view angle. In each image, the plume area was estimated on the basis of the area covered by waters with high nLw555 backscattering index. The level of nLw555 index to distinguish between the plume and the ambient waters was initially unknown; the goal of the study was to select the nLw555 index which best characterizes the plume boundary. For this, the "plume boundary" threshold levels were tested within the range from 0.5 to 2.0 $mW\,cm^{-2}\,\mu m^{-1}\,sr^{-1}$. The mean nLw555 was also calculated within the rectangle 33.47°N–33.79°N; 118.4°W–117.7°W (see Fig. 2) from both Level 2 and Level 3 SeaWiFS data. Daily Level 3 Standard Mapped Images (SMI) L555 data (i.e., the global grids of 360°/4096 pixels spatial resolution

containing nLw555 collected during each day of observations) were obtained from GSFC DAAC ftp site ftp://samoa.gsfc.nasa.gov/pub/sdps/V4/L3SMI. The data from the rectangle 33.47°N–33.79°N; 118.4°W–117.7°W (total 14 pixels) were extracted from global grids and averaged. In SeaWiFS Level 3 L555 files the value $1.275\,\mathrm{mW\,cm^{-2}\,\mu m^{-1}\,sr^{-1}}$ indicates MD; all these values were replaced by MD code before averaging.

Rainstorm magnitude was estimated from the atmospheric precipitation averaged over the Dominguez Channel, Los Angeles River, San Gabriel River, and Santa Ana River watersheds (Fig. 1). Daily rain gauge data from 38 meteorological stations located in these watersheds were downloaded from the NOAA National Data Center Climate Data Online (NNDC/CDO) Internet site. Each observation represents the precipitation during a 24-h period preceding the observation time. The precise time of observation varied between the stations during different periods; therefore, each observation was attributed to an entire day and the variability at a sub-diurnal time-scale was not analyzed. Not all stations had continuous data for the entire 6-year period of analysis; therefore, the average precipitation for each day from September 1997 till June 2003 was estimated from a variable number of stations.

The analysis of correlation between the rainstorm and the plume area is based on the model of linear "signal/response" dependence between these two parameters. To obtain a quantitative statistical evaluation of the response of the plume size as estimated by an area occupied by water with nLw555 exceeding the selected threshold to the rainstorm signal, the time-lagged linear Pearson correlation coefficients between the plume area and the rainstorm magnitude were estimated. Different levels of nLw555 were used to find maximum correlation between plume area and rainstorm; the nLw555 resulting in maximum correlation was considered as the best plume edge indicator.

To evaluate the persistence of the rainstorm signal in the plume area, we estimated for each (t-th) day the precipitated water volume (V_t) accumulated during the previous period by the day preceding the plume, using the equation:

$$V_t = \sum_{i=1}^{t-1} k^{t-i} P_i = P_{t-1} + kP_{t-2} + k^2 P_{t-3} + k^3 P_{t-4} + k^4 P_{t-5} + \ldots, \quad (1)$$

where P_i is the precipitation during the i-th day and k is the coefficient of persistence of the freshwater plume. The meaning of k ($0<k<1$) is that during each day the k-th part of the water accumulated during the preceding period is retained in the plume and the (1-k)th part is dissipated. The values of k within the range from 0.05 to 0.95 were tested to obtain best correlation between V_t and the plume area.

To analyze the effect of antecedent storms on plume size, we selected the observations when the rainstorm and the resulting plume followed a dry period. For this, events were selected when the precipitation during the 7-day period preceding the rainstorm did not exceed 2.5 mm. The latter value was selected because earlier it was indicated as a threshold under which no rainfall effect was observed in the coastal beaches (Ackerman and Weisberg, 2003).

To study the influence of local circulation on plume dynamics, two indices were estimated for each plume: (1) the residual of linear regression between the plume area and the main factor regulating its size (i.e., the accumulated precipitation), and (2) the index of alongshore translocation. The latter was defined as the ratio between the parts of the total plume area to the west and to the east of 118.10°W (near the mouth of the San Gabriel River, see Fig. 2); the latter longitudinal coordinate was selected arbitrary as a center of the plume typical to San Pedro Basin. The dynamics of the "plume residuals" and "plume translocation" indices were analyzed in terms of correlation with the wind stress at different locations along the North American coast and with the tidal variability related to lunar cycle.

Wind data were obtained from the National Center for Environmental Prediction (NCEP); the global wind data are supplied by the NASA GSFC DAAC as ancillary information for SeaWiFS users. These files contain regular grids of zonal

and meridional wind speeds at 10 m above the earth surface interpolated on an equidistant cylindrical projection of 1° spatial resolution and 6-h temporal resolution (12-h during some periods in 1998 and 1999). The zonal and meridional wind speeds were transformed to the alongshore equatorward and onshore wind stress ($kg\,m^{-1}\,s^{-2}$) using the conventional equation $\tau = C_d\rho_a|U|U$, where U is wind speed ($m\,s^{-1}$), ρ_a is air density ($1.2\,kg\,m^{-3}$), and C_d is the dimensionless "drag coefficient" (0.0013). The coastline angles are given in Table 1. We analyzed the correlation between the plume area and the alongshore equatorward and onshore wind stress between 23°N and 34°N along the North American coast during the entire period of observations (from October 1997 to June 2003). Before estimating correlation coefficients, the "plume residual" and the "plume translocation" indices and the wind stress were smoothed using a 7-day filter window.

The tidal variations were estimated by the model XWTide32 obtained from the Internet site http://XWTide32.com. The sea elevations were estimated with 1-h time step at the Long Beach Terminal Island (33.451°N, 118.136°W) during 1997–2003. The tidal variability related to lunar cycle was estimated as a standard deviation of sea surface elevation during each day of lunar cycle. To examine the hypothesis of the influence of tidal amplitude on the freshwater plume area, the "plume residuals" were plotted against the day since the full moon following an approach used by Pineda (1995).

Table 1
The locations along the North American Pacific coast where the alongshore equatorward and onshore wind stress were estimated

Latitude	Longitude	Angle
34°N	119°W	70
33°N	118°W	40
32°N	117°W	25
31°N	117°W	30
30°N	116°W	20
29°N	115°W	50
28°N	115°W	30
27°N	115°W	40
26°N	114°W	50
25°N	113°W	30
24°N	112°W	45
23°N	111°W	25

The angle is between the north-south direction and the coastline.

4. Results

The optical properties of the ocean surface over the San Pedro Shelf dramatically changed after episodic winter rainstorms. The zone of increased sediment concentration (i.e., the plume) can be observed along the coast immediately following the storm. During subsequent days, this zone is transformed by local circulation and gradually dissipates. Fig. 3 illustrates the most pronounced plume observed at the end of February 1998 during torrential rains in southern California (4.2–6.1 cm/day during three days from 02/23/98 to 02/25/98) related to the 1997–1998 El Niño event. During other winter seasons, the rainstorms were not as heavy and the resulting plumes were not as large (Fig. 4).

The analysis of the statistical relationship between the signal (rainstorm) and the response (plume area) includes two issues: first, the estimation of the nLw555 level that best characterizes the plume boundaries; and second, the evaluation of the time lag between the rainstorm and the plume. Different values of the nLw555 level and the time lag were tested to achieve an optimal relationship (i.e., maximum correlation). The linear correlation coefficients were calculated between rainstorm and plume, testing 0–15 days time lag of precipitation prior to the plume. The boundaries of the plume areas were estimated from nLw555 within the range from 0.5 to $2.0\,mW\,cm^{-2}\,\mu m^{-1}\,sr^{-1}$ (Fig. 5). The best correlation was observed at a 1-day time lag, i.e., the day immediately following the rainstorm event. As the time lag increased, the correlation gradually decreased. As for the nLw555 level indicating the plume boundary, values from 1.0 to $1.9\,mW\,cm^{-2}\,\mu m^{-1}\,sr^{-1}$ resulted in similarly high correlation coefficients (from $+0.50$ to $+0.54$, maximum at $nLw = 1.6\,mW\,cm^{-2}\,\mu m^{-1}\,sr^{-1}$).

Atmospheric precipitation in the study area was well autocorrelated (about $+0.50$) at the one-day

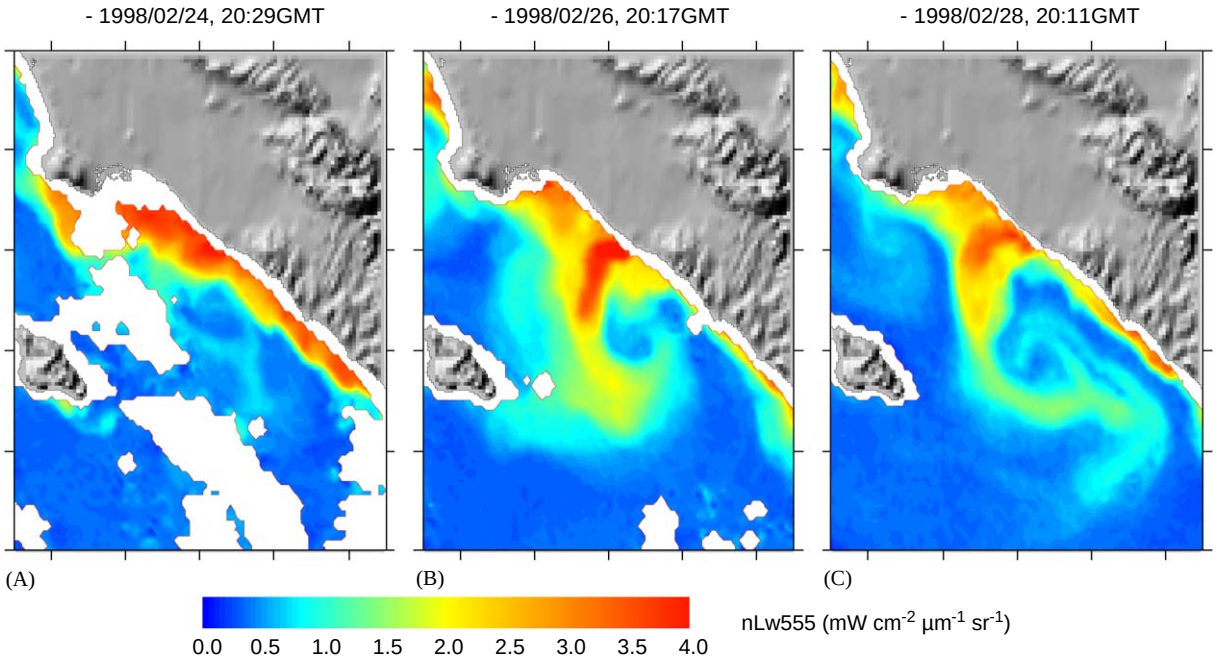

Fig. 3. SeaWiFS images of stormwater runoff plumes along the San Pedro Shelf during February 24 (A), 26 (B) and 28 (C) 1998.

time lag only; at other time lags, the correlation was very small (Fig. 6A). The plume area, in contrast, exhibited much more persistent signal (Fig. 6C); the correlation at one-day time lag was +0.91 and gradually decreased with time lag (+0.49 at 10-day time lag, +0.32 at 20-day, etc.). To improve consistency in the autocorrelation functions of rain and plume, we transformed precipitation to accumulated rain using Eq. (1). After transformation of the precipitation time-series to accumulated precipitation, the autocorrelation function of the latter (Fig. 6B) appeared to be similar to the autocorrelation function of the plume area (Fig. 6C).

The correlation of the plume area to the accumulated rainwater was analyzed by testing the correlation between these two parameters varying nLw555 values and the coefficient of persistence k in Eq. (1). There was an evident maximum (correlation coefficient = +0.85) at nLw555 = 1.3 mW cm^{-2} µm^{-1} sr^{-1} and $k = 0.75$ (Fig. 7). The correlation was almost linear (Fig. 8); the plume area during t-th day (S_t, km^2) can be estimated from the precipitation (P_t, mm/day) by the equation

$$S_t = 1.3 + 82.4^* V_t, \quad (2)$$

where P_t is transformed to V_t by Eq. (1). The regression summary and the analysis of variance of the relationship between S_t and V_t are given in Table 2. The regression equation is highly significant. Nevertheless, some rainstorms of 3–4 cm of accumulated rainfall produced no plumes; at the same time, very small rainfalls sometimes coincided with plume areas by 200–400 km^2. However, the intercept of the linear Eq. (2) is very small and insignificantly different from zero, indicating that even small rainfalls reach ocean and produce plumes. The coefficient of determination (R^2) is 0.725.

To test the hypothesis that antecedent storms influence the relation between plume size and precipitation, storm events following a 7-day dry period were selected. The relation between precipitation and plume size did not differ from the entire data set. The coefficients of the linear

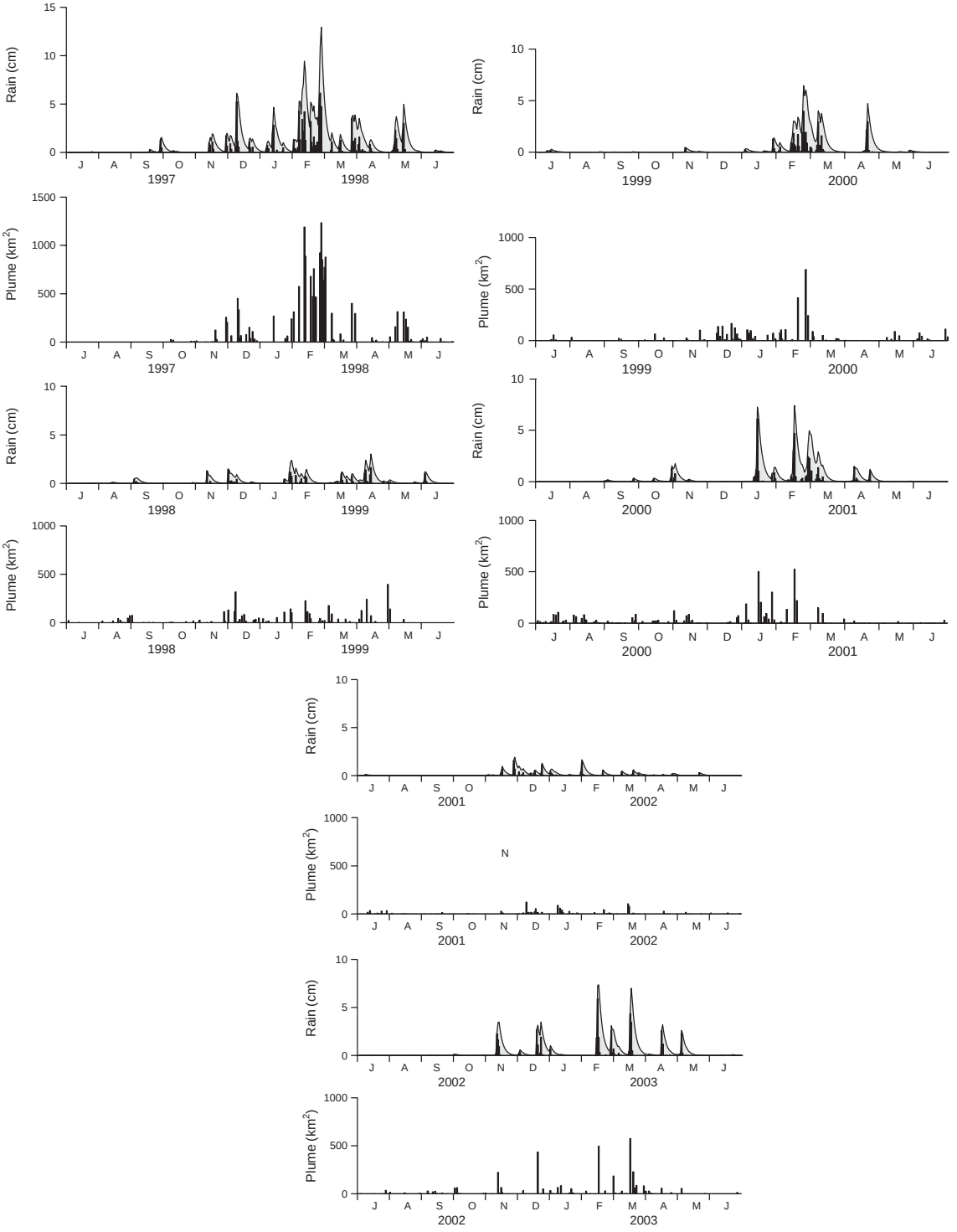

Fig. 4. Rainstorm magnitude (daily and accumulated with $k = 0.75$) and the plume areas during September 1997–June 2003.

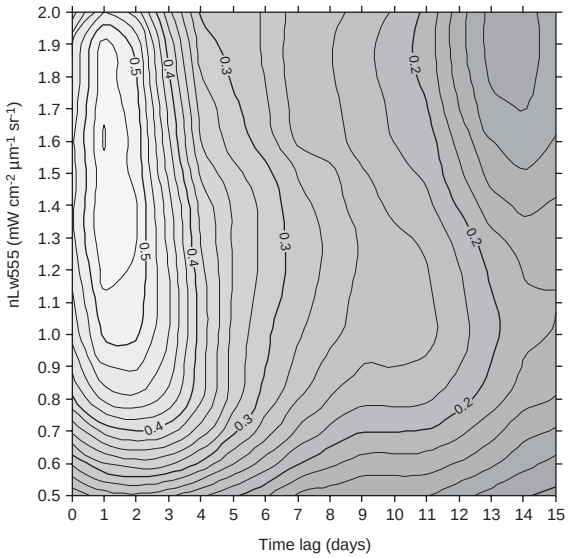

Fig. 5. 2D-diagram of the correlation between the freshwater plume area (bounded by different nLw555 levels) and the rainstorm magnitude at different time lags.

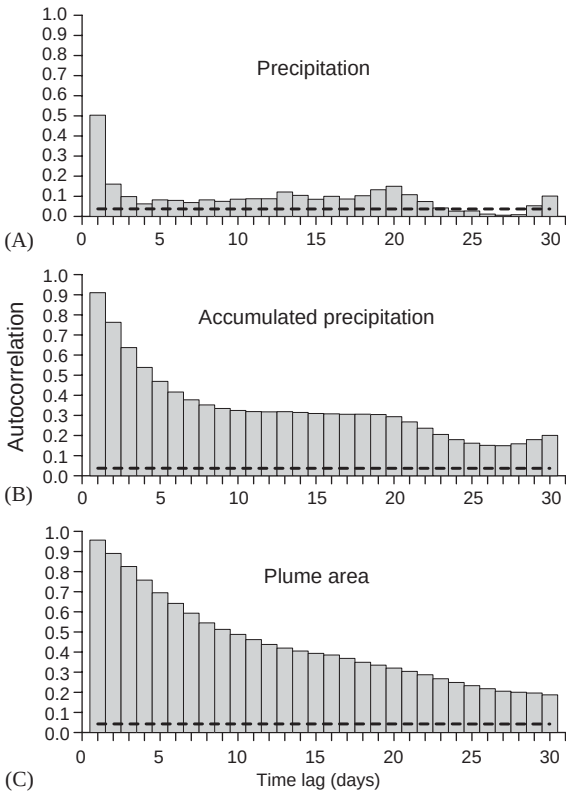

Fig. 6. The autocorrelation functions of the atmospheric precipitation over the watersheds producing freshwater discharge to the San Pedro Shelf (A); the precipitation accumulated with Eq. (1) (coefficient of persistence $k = 0.75$) (B); the freshwater plume area bounded by nLw555 = 1.3 mW cm^{-2} µm^{-1} sr^{-1}. Dashed lines indicate 95% confidence levels.

equation (intercept = 14.3 and slope = 75.23) were insignificantly different from the coefficients of Eq. (2).

The plume areas in 494 of 628 images (79%) were $<50\,km^2$; only 75 plumes (12%) exceeded $100\,km^2$ (Fig. 9). Maximum plume size estimated on the basis of nLw555 $>1.3\,mW\,cm^{-2}\,\mu m^{-1}\,sr^{-1}$ exceeded $1000\,km^2$; these plumes were observed in February 1998 during a strong El Niño event (Fig. 3).

The influence of local circulation on plume dynamics was analyzed on the basis of the time-lagged correlation between the "plume residuals" (i.e., the residuals of Equation 2) and "plume translocation" to the onshore and alongshore equatorward wind stress at different locations (from 34°N to 23°N) along the North American Pacific coast (Figs. 10 and 11). As for onshore wind stress, none of the correlation coefficients with both indices (plume size residuals and alongshore plume translocation) were significant.

The correlation between plume area residuals and the alongshore equatorward wind stress was weak, but significant. A small positive correlation (+0.07) was observed between the plume residuals and the wind stress at 32°–33°N with time lag from 2 to 9 days (Fig. 10). With wind stress further to the south, the correlation changed to negative, with two extremes, at 28°N (time lag 1–2 days) and 23°N–25°N (time lag 1–4 days). The signs of these extremes indicated that the local wind forcing (at 32°–33°N) produced circulation slightly increasing the plume area. The remote wind forcing from the central part (and especially from the southern tip) of Baja California slightly decreased the freshwater plume. The coefficient of determination R^2 was very small (<0.01). Including new variables into the linear regression Eq. (2) (see Table 2) did not increase its significance.

The correlation between plume "westward" translocation and the equatorward wind stress

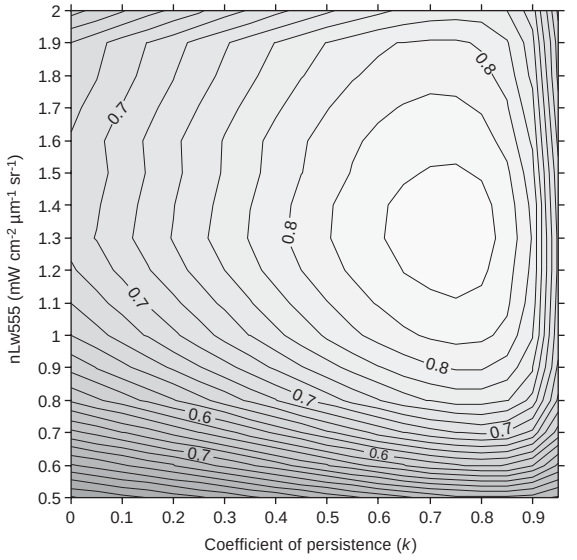

Fig. 7. 2D-diagram of the correlation between the freshwater plume area bounded by different nLw555 levels (*Y*-axis) and the accumulated precipitated water estimated with different coefficient of persistence (*k*, *X*-axis).

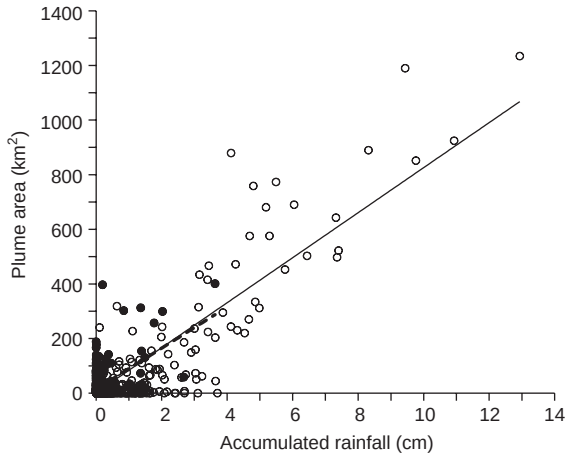

Fig. 8. The correlation between the accumulated precipitated water ($k = 0.75$) and the freshwater plume area bounded by $nLw555 = 1.3\,mW\,cm^{-2}\,\mu m^{-1}\,sr^{-1}$. The plumes observed after 7-day dry period are marked by solid circles and dashed fitting line.

(Fig. 11) was higher than the correlation between plume area residuals and wind. The most prominent correlation (about −0.21) was observed between the plume position and the equatorward wind stress at 29–30°N at the time lag between 0 and 2 days. The resulting coefficient of determination R^2 was 0.044. The negative sign of the correlation coefficient indicated that the increase of the equatorward wind stress along the central Baja California resulted in slight equatorward (i.e., eastward) translocation of the plume; on the contrast, the decrease of the equatorward wind stress resulted in poleward (westward) plume translocation. In other words, the direction of remote wind forcing coincided with the direction of the alongshore translocation of the plume.

To examine the influence of tidal circulation on the plumes, we correlated the residuals of the plume area not explained by the accumulated precipitated water (see Eq. (2)) with the tidal variability, which in the Southern California Bight depends mostly on the lunar cycle (Fig. 12). The correlation between the residuals of the plume area and tidal variability was very low and statistically insignificant ($r = 0.07; p = 0.062$). Including tidal variability as a new variable into the linear regression Eq. (2) (see Table 2) did not increase its significance. Averaging the residuals of the plume area over the day of lunar cycle reveals a slight relationship: maximum positive residuals were observed during the 16–17th and 28–29th days of lunar cycle (see the bar chart at Fig. 12A), meaning that during the periods of maximum tidal variability (i.e., new moon and full moon) the plume area was more "washed out" as compared with other periods of tidal cycle. This relationship was too small to be statistically significant ($p = 0.062$ rather than the conventional 0.050 confidence level).

5. Discussion

5.1. Satellite ocean-color derived backscattering index nLw555 as robust plume indicator

The high linear correlation ($R^2 = 0.725$) we observed between the plume areas estimated using the nLw555 threshold level and accumulated precipitation (see Eq. (2)) suggests that normalized water-leaving radiance ($nLw555 = 1.3\,mW\,cm^{-2}\,\mu m^{-1}\,sr^{-1}$) is a good proxy of

Table 2
Regression summary and the analysis of variance of the linear correlation between the accumulated rainwater (X) and the plume area size (Y).

$N = 628$	β (standardized regression coefficients)	Standard Error of β	B (regression coefficients)	Standard error of B	$t(626)$	p-level
Intercept			1.34007	3.164553	0.42346	0.672102
X	0.851591	0.020952	82.43676	2.028175	40.64579	0.000000

Effect	Sums of squares	d.f.	Mean squares	F	p-level
Regression	8,739,009	1	8,739,009	1652.080	0.0000
Residual	3,311,353	626	5,290		
Total	12,050,362				

Correlation coefficient $R = 0.85159098$; coefficient of determination $R^2 = 0.71520719$.

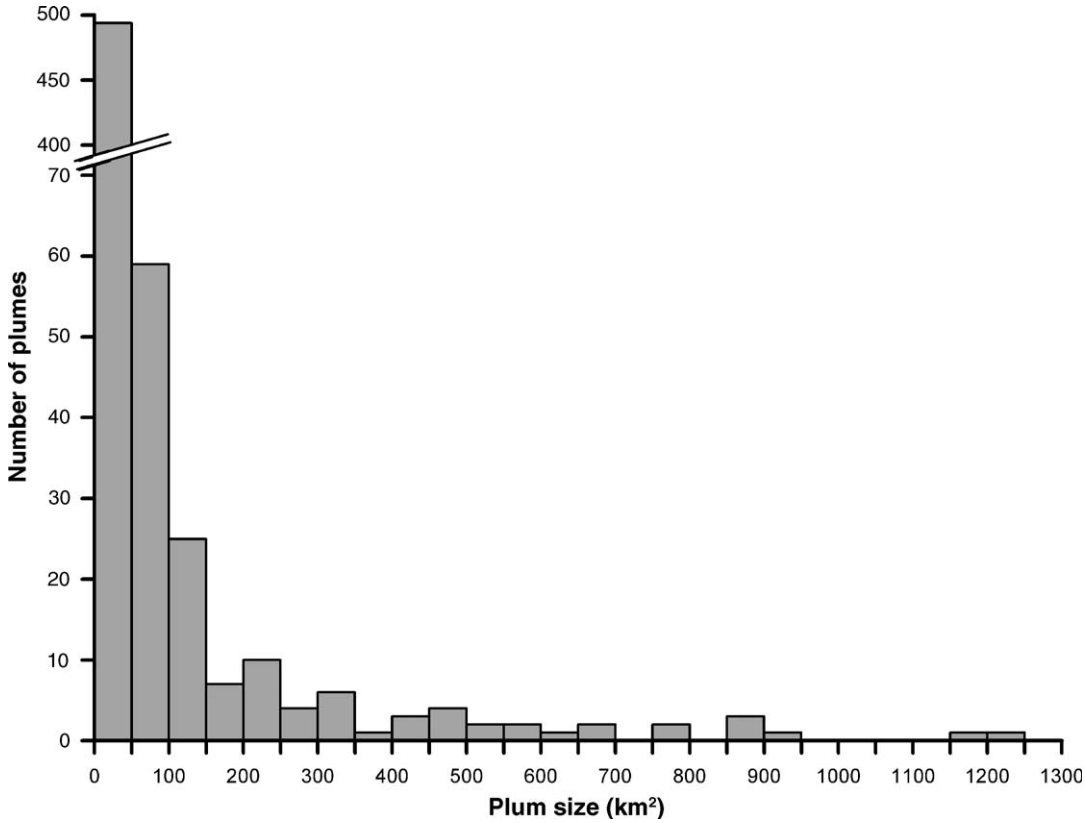

Fig. 9. Size frequency distribution of plumes areas observed over the San Pedro Shelf during September 1997–June 2003 (total 628 images).

freshwater plume size along the San Pedro Shelf. A similar nLw555 value was found for the Santa Barbara Channel by Otero et al. (2001). This significant backscattering value indicates turbid waters with high loadings of suspended matter that likely resulted from episodic freshwater runoff,

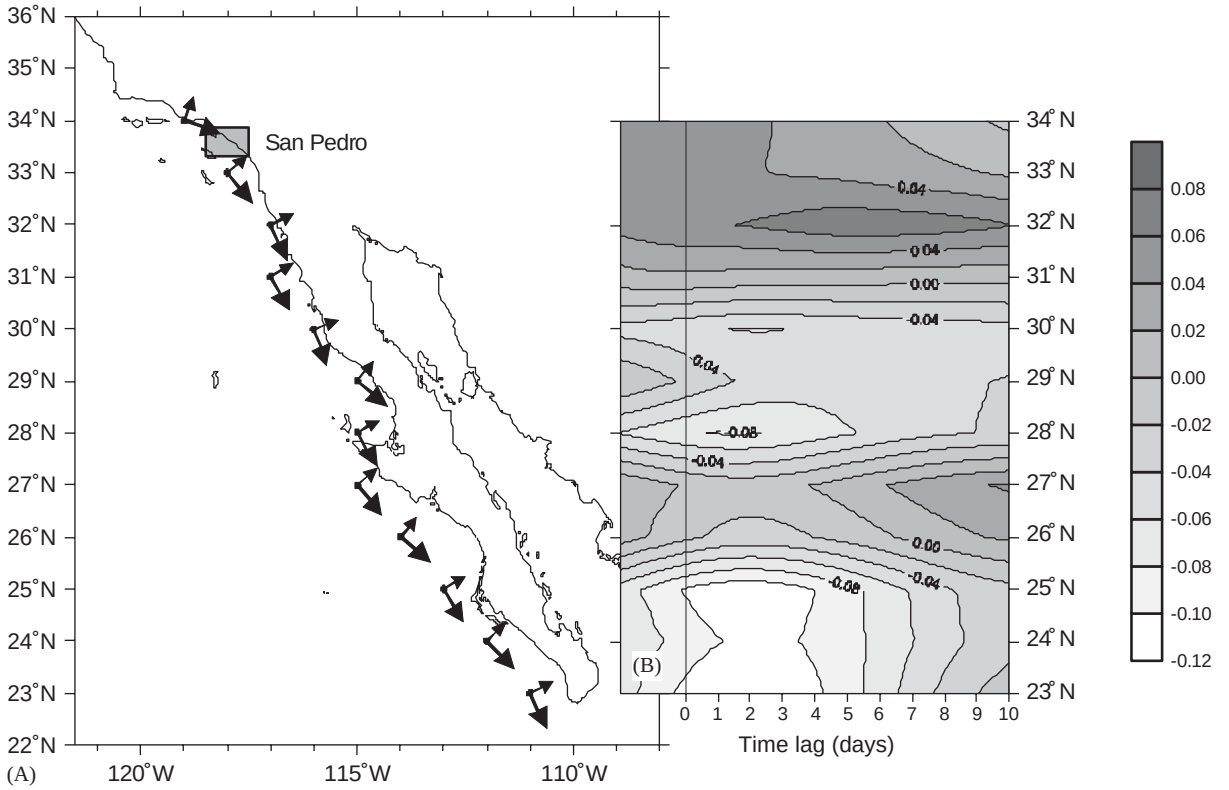

Fig. 10. The locations of the NCEP wind grid nodes used for the analysis of remote forcing (A); the San Pedro area is marked with a rectangle; 2D diagram of correlation between the equatorward wind stress and the residuals of plume area not explained by the accumulated precipitated water, Eq. (2) (B).

which, in turn, were presumably associated with elevated concentrations of pollutants, contaminants, bacteria and viruses, etc. Further studies are needed to establish the linkages between these geophysical and ecological parameters.

The high linear correlation (the coefficient of determination $R^2 = 0.793$; Fig. 13a) between the areas of freshwater plumes estimated from the optical signature with nLw555 $> 1.3\,\mathrm{mW\,cm^{-2}\,\mu m^{-1}\,sr^{-1}}$ and the nLw555 index averaged over the entire San Pedro Basin zone (33.47°N–33.79°N; 118.4°W–117.7°W) suggests that the total value of nLw555 averaged over this study area ($\sim 35 \times 65$ km) can be used to estimate plume size in time-series analysis. Such a high correlation provides promise for using lower-resolution remote sensing to retrospectively study plume dynamics. In this work, we estimated the plume areas from high-resolution (1.1-km) satellite images, which is a time and labor-intensive process. Level 3 nLw555 data processed at GSFC are highly correlated (the coefficient of determination $R^2 = 0.7833$) with Level 2 data we processed from Level 1 data using SeaDAS software. However, this correlation is logarithmic rather than linear (Fig. 13b; $L3 = 0.4900^{*}\ln(L2) + 0.7988$). The apparent reason of this non-linearity is that in the Level 3 data all high values of nLw555 , i.e., $> 1.275\,\mathrm{mW\,cm^{-2}\,\mu m^{-1}\,sr^{-1}}$ (often resulting from atmospheric correction issues), were replaced by MD. This should be taken into account in future time series analysis of freshwater plumes utilizing lower-resolution, e.g., Level 3 SeaWiFS (9-km) and MODIS (4.5-km) Standard Mapped Images (SMI) satellite data, available through the NASA GSFC DAAC. Processing Level 3 SMI files requires much less

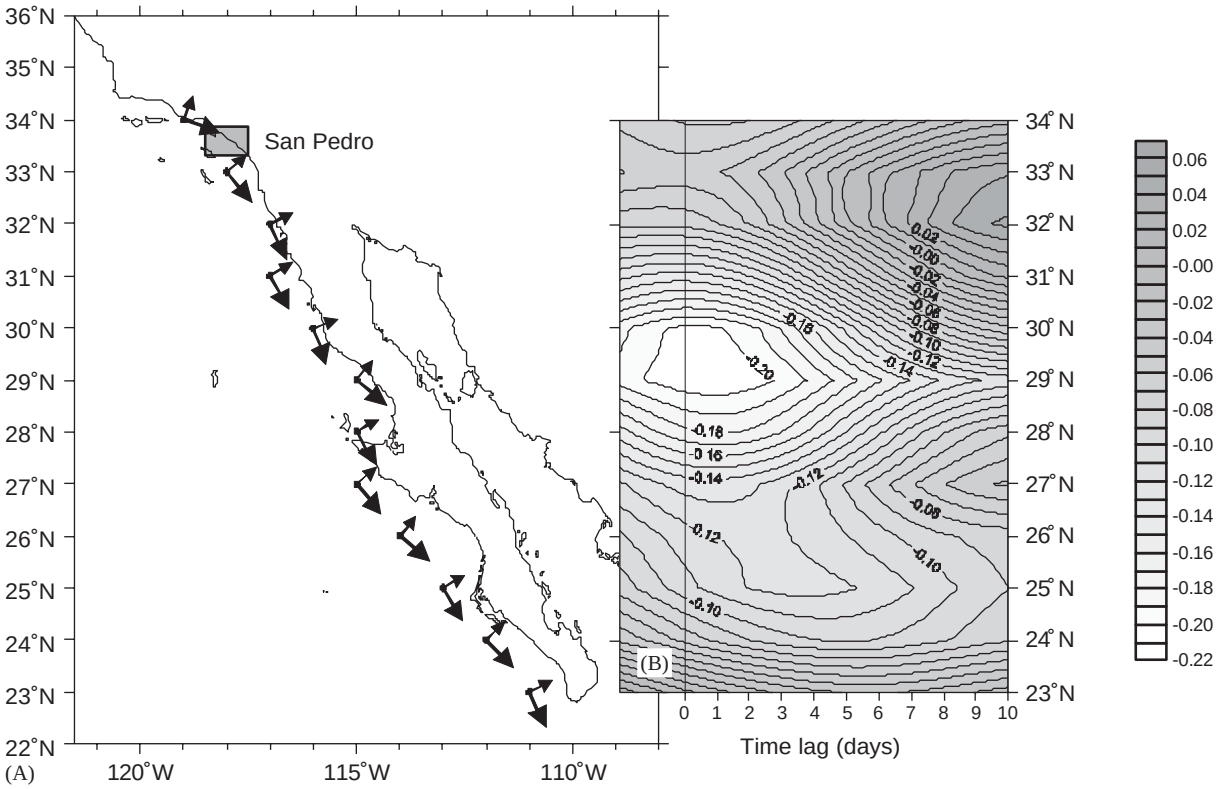

Fig. 11. The locations of the NCEP wind grid nodes used for the analysis of remote forcing (A); the San Pedro area is marked with a rectangle; 2D diagram of the correlation between the equatorward wind stress and the index of alongshore translocation of the plume (the percentage of the plume located to the west of 118.1°W) (B).

work than Level 1 or 2 (~1-km) and the data from many areas of interest (e.g., the entire coast of southern California) can be extracted quickly from all files of the multi-year data set and converted into a time-series, which can then be analyzed using appropriate statistical methods. This analysis would facilitate the statistical prediction of the effect of large-scale and/or lower frequency (e.g., interannual) meteorological and oceanographic factors (e.g., El Niño) on plume size. However, in support of local pollution assessment activities and real-time monitoring and decision-making needs (e.g., beach closures), even higher resolution ocean color imagery in both time (e.g., sub-diurnal) and space (<500 m) is required to adequately observe and predict event-scale plume variability and attendant ecological impacts.

5.2. The correlation between the plume area and the amount of precipitated water

The "accumulated rainwater" index estimated from rainfall using Eq (1) (3/4 accumulated and 1/4 dissipated daily) is recommended for use in coastal management (e.g., beach closure decisions) instead of 1-day rainstorm magnitude, because it much better predicts the plume area (the coefficient of determination $R^2>70\%$). The plumes along the San Pedro Shelf appear immediately after the rainstorms and persist for several days, if not weeks. Rainfall during the day prior to the plume contributes most significantly to the plume; however, solely taking into account this "last day" of precipitation only explains as little as 30% of the plume size. Hence, precipitation that occurs during the preceding period of several days (and

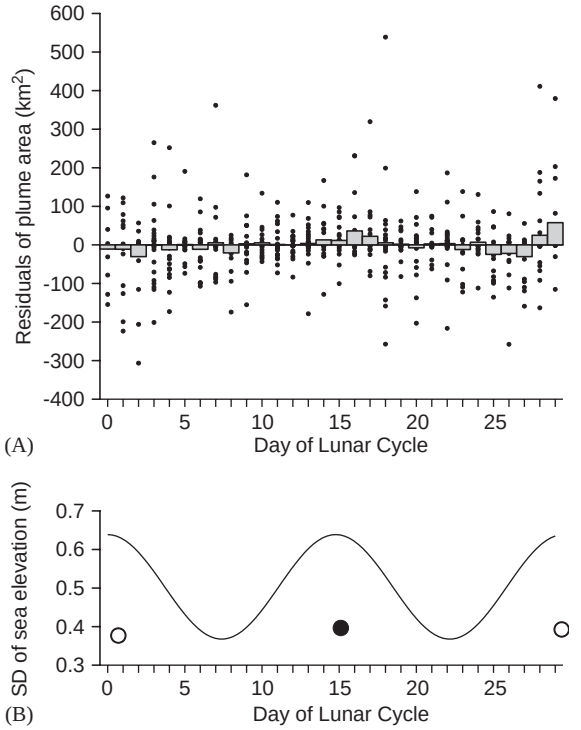

Fig. 12. The residuals of freshwater plume area not explained by the accumulated precipitated water (Eq. (2)) vs. tidal cycle (A); the bar chart represents the residuals averaged over the day of tidal cycle. The intensity of tidal cycle (B) is represented as a standard deviation of the sea surface elevation during each day of lunar cycle; open circles indicate full moon; solid circle indicates new moon.

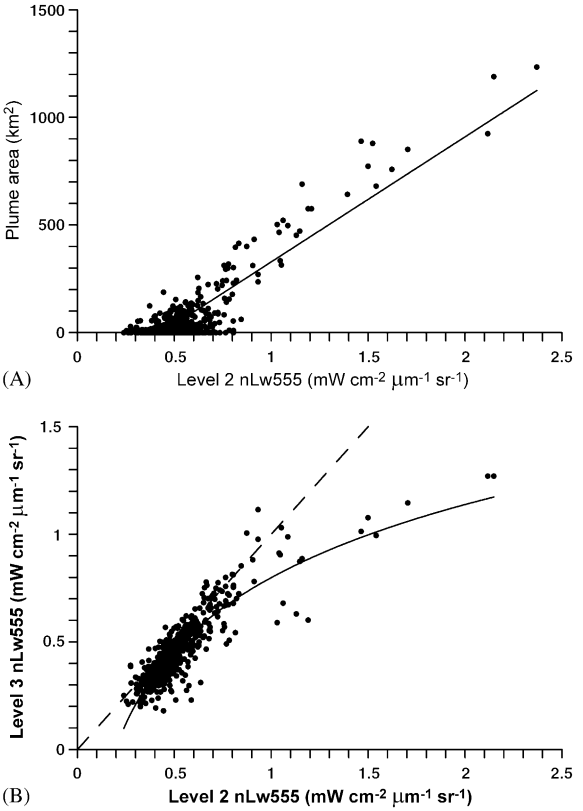

Fig. 13. (A) The correlation between the nLw555 averaged over the San Pedro Shelf and the freshwater plume area bounded by $\mathrm{nLw555} = 1.3\,\mathrm{mW\,cm^{-2}\,\mu m^{-1}\,sr^{-1}}$; (B) The correlation between the nLw555 averaged over the San Pedro Shelf obtained from Level 2 and Level 3 SeaWiFS data.

sometimes weeks) rather than the single last day of rain should be taken into account by coastal decision-makers.

The zero intercept correlation between S_p and V_t (Fig. 8) indicates that even small precipitation resulted in a plume. It also suggests that almost all rainwater precipitated over the watersheds of Dominguez Channel, Los Angeles, San Gabriel, and Santa Ana rivers was discharged to the coastal ocean and formed the plume. The portion of infiltrated water was apparently very small. We assume that the fresh water discharged into the coastal ocean spreads horizontally, the vertical structure of the plume being characterized by highly stable stratification (Garvine, 1982; Chao and Boicourt, 1986; Garvine, 1987; O'Donnell, 1990; Fong and Geyer, 2001; Pritchard and Huntley, 2002). In the most primitive model, the vertical extension of the plume water can be roughly assumed as a constant. The volume of low salinity water producing the plume (V_p) is the plume area (S_p) times the plume depth (H); it is proportional to the total volume of precipitated water accumulated in the watershed, which is the accumulated precipitation estimated by Eq. (1) (V_t) times the constant watershed area (S_w).

$$V_p \sim S_p * H \sim V_t * S_w. \tag{3}$$

H and S_w are constants; hence, the plume area S_p is proportional to the accumulated precipitated water V_t and the correlation between S_p and V_t should be linear; this theoretical concept is corroborated by our observations (Fig. 8). The

total catchment area of four watersheds is 9320 km^2; the coefficient of Eq. (2) transforming the accumulated rainwater (mm) to plume area (km^2) is 82. Hence, the ratio between the total watershed area and the area of the plume produced by 1 mm of rainfall is about 100:1. Washburn et al. (2003) indicate the salinity in runoff plumes in the Southern California Bight is <32.9 PSU; the mean ambient salinity in this area can be roughly assumed as 33.6–34.0 PSU (Hickey, 1993). As such, the difference between the salinity in the plume and in the ambient seawater is >1. Under these assumptions, the plume depth cannot exceed 3.5 m. Mertes and Warrick (2001) indicate the thickness of the plume from the Santa Clara and Ventura rivers in the northern part of the Southern California Bight varies from 5 m in the zone of highest concentration of Total Suspended Matter (TSM) to 1.5 m at the plume boundary; Washburn et al. (2003) note similar plume depths in the Santa Monica Bay. These measurements of plume depth correspond well to data reported for other rivers (Geyer et al., 2000) and model results (Chao, 1998). An assumption that in this study area not all rainwater flows to the ocean to form the plume results in the estimation of the plume depth <3.5 m, which contradicts the earlier observations. Indeed, the thickness of plumes is not a constant. Nevertheless, including a constant slope into Eq. (3) makes it more complex but does not change the conclusion that along the San Pedro Shelf almost all runoff flows unimpeded to the ocean.

The short time lag between rainstorms and plumes is consistent with the nature of the watersheds in the study area: they are highly impervious, have little storage, and are characterized by a short distance between the top of the watershed and the coast. Numerous flood control reservoirs with dams (see Ackerman and Schiff, 2003) do not retain much rainwater, which flows unimpeded to the ocean. The speed of stormwater runoff in the Los Angeles River can reach 45 mph (70 km/h) (Gumprecht, 1999). A nearly immediate linear response of freshwater runoff to rainstorm >0.9 mm was noted by Ackerman and Weisberg (2003) in the watershed of the Ballona Creek, and by Reeves et al. (2004) in the Talbert watershed, adjacent to the study area. Such rapid runoff is common in watersheds with a high percentage of impervious surfaces (Arnold and Gibbons, 1996; Beighley et al., 2003; Vaze and Chiew, 2003). The discharge in these areas can result in high bacterial contamination of the coastal waters following storms (Mallin et al., 2000).

We also tested the hypothesis that antecedent stormwater concentrated in the ground decreases the infiltration rate in the watersheds, which, in turn, increases runoff and plume size. However, no difference was revealed between the entire data set and the rainstorms following a 7-day or longer dry period. We conclude that in the developed urbanized watersheds of southern California the variation of infiltration rate is small as compared with other factors influencing freshwater discharge (primarily the rainstorm magnitude).

5.3. *Factors influencing plume dynamics*

The amount of precipitation over the watershed was the main factor regulating the plume area over the San Pedro Shelf. The influence of other factors on the plume dynamics, such as tides and the coastal circulation, was relatively small.

The correlation between the plume area and the tidal amplitude was small and insignificant. The daily averaged range of tidal variability in the Southern California Bight varies between 0.1 and 2.0 m. As noted in other coastal regions (Stumpf et al., 1993; Pritchard and Huntley, 2002), we expected that along the San Pedro Shelf the tidal currents can influence the plume area, since a stronger range of tidal circulation can enhance the spreading of the plumes. Previous studies have indicated the influence of the range of tidal circulation on the coastal pollution in the recreation areas of southern California (Boehm et al., 2002a,b). However, over the San Pedro Shelf, the influence of spring tides on plume dispersion was subtle. One explanation is that in this study, we analyzed only large freshwater plumes due to the spatial resolution of the satellite images (pixel size $\sim$1 km). These large plumes are not influenced by local tidal circulation. Another explanation is that in our study variations of sea surface elevation were analyzed rather than the

horizontal circulation induced by the tides. According to the observations of Winant and Bratkovich (1981), at the shelf of southern California neither cross-shelf nor alongshore tidal currents are well correlated with the tidal elevation of sea surface; so, the influence of tidal variability on the plumes is too complex to be resolved by a primitive tidal model.

No dominant pattern of plume propagation was revealed. After heavy rainstorms, the zone of highest ocean surface backscattering index (nLw555) was located from Palos Verdes to the southeast along the shore (Fig. 3A). The freshwater discharge from different watersheds often commingled in the nearshore zone, making it impossible to analyze these plumes separately. The size of the collective plume varied due to rainstorm magnitude. During the days following each storm, the local circulation transformed the plume in different ways. Most typically, there was an offshore and southward propagation of the plume with its leading edge bending inshore in a counterclockwise direction (Fig. 3), resembling cyclonic eddy recirculation. These observations appear consistent with previous findings from this region. Warrick et al. (2004) note that in southern California the plumes produced by the annual peak discharge are strongly influenced by river intertia, producing jet-like structures ~10 km offshore. Regarding the recirculation patterns, Burkov and Pavlova (1980) reported that most of the eddies located inshore of the mainstream of the California Current are cyclonic. DiGiacomo and Holt (2001) studied the eddies in the Southern California Bight and discovered that most (~94%) of the eddies had cyclonic rotation. Further, the San Pedro Basin is an area where these eddies are concentrated.

No preference in the direction of plume propagation (i.e., poleward or equatorward) was revealed. This result prima face contradicts to the theoretical concept that in the northern hemisphere the propagation of the freshwater plume should be directed to the right (Chao and Boicourt, 1986; Garvine, 1987; Yankovsky et al., 2001). However, the plumes off southern California should be classified as small scale river plumes in which the influence of planetary rotation, as estimated by comparing the characteristic plume scale to the internal Rossby deformation radius, is of secondary influence (O'Donnell, 1990). Therefore, the role of synoptic scale meteorological forcing on the trajectory of the plume is more important than in large river systems (Geyer et al., 2000). However, local winds do not influence the plume; this conclusion is based on insignificant correlation in Figs. 10 and 11 and agrees well with the statement that the local atmospheric forcing on the circulation in the Southern California Bight is weak (Winant and Bratkovich, 1981; Hickey et al., 2003). We detected a subtle influence of local circulation on the alongshore translocation of the plumes; this circulation was induced by the remote wind forcing a few hundred kilometers to the south at the Baja California coast (29°–30°N). This influence was very small and explained only 4–5% of the alongshore plume variability. A similar correlation was detected between the alongshore winds to the south and water temperature off southern California by Pringle and Riser (2003) near San Diego (maximum correlation with the wind at 29°–30°N, the wind 1–2 days leading the temperature) and by Boehm et al. (2004) near Huntington and Newport Beaches (wind at 27.5°N leading temperature by 1 day). The mechanism of remote influence of wind stress on the circulation in the Southern California Bight was also described by Hickey et al. (2003). These authors observed maximum correlation between the local circulation and the wind at 25°–30°N with a time lag of few days and attributed this influence to the alongcoast propagation of low-mode (>10-day period) coastally trapped waves. Each coastally trapped wave is a result of strengthening of the equatorward wind at Baja California coast, resulting in Ekman offshore drift and upwelling, which propagate poleward due to Coriolis force. However, the correlation between these waves and the plumes in the San Pedro Basin is weak. One possible explanation is the local bottom topography: the San Pedro Shelf, especially its western part, is wide compared to other parts of the southern California coast (Fig. 2); a shallow bottom can damp the influence of coastally trapped waves. This can partly explain why equatorward winds off Baja California result in eastward plume translocation: the pulses of offshore flow induced by the coastally trapped waves

shifted the plume to the deeper eastern part of the San Pedro Shelf, slightly decreasing the plume size.

Over shallow depths of the San Pedro Shelf, alongshore circulation was weak and did not exert much influence on the freshwater plumes, because in this area the speed of alongshore currents increases offshore (Winant and Bratkovich, 1981; List et al., 1990). However, in other areas of southern California the shelf is narrower and the influence of the coastal circulation on the plumes may be more pronounced.

5.4. Summary and future directions

Difficulty in predicting the extent and direction of contaminant-laden freshwater runoff plumes is an important problem for coastal management. This study focused on characterizing runoff dynamics from heavily populated and developed coastal watersheds and in this context should provide significant insights into water quality issues in other urban coastal regions. In particular, from this study it is clear that the greater the accumulated precipitation, the greater the plume extent will be along the San Pedro Shelf. However, we failed to establish a clear correlation between the plumes and the wind pattern because the statistical model we used was too primitive. Improved synoptic, regional wind and/or surface current fields (e.g., from shore-based high frequency radar arrays and direct measurements of coastal circulation from moored sensors) would improve our ability to assess and predict the complex transport of plumes and associated loadings. In particular, plume spatial variability often results from the interaction between the coastal plume and near-shore (sub) mesoscale processes such as cyclonic eddies. As a result, the plume water is entrained in the orbital circulation and transported alongshore (mainly poleward) and/or offshore, depending upon the location of the eddy and the direction of its propagation. Thus, the resulting change of the shape of the plume is related directly to local circulation, but the influence of the coastal circulation on the contaminant transport is noticeably non-linear; this topic will be a focus of our upcoming studies. The methodological approach will include a combination of non-linear statistical analysis, estimation of (sub) mesoscale circulation from the series of satellite images, and numerical modeling. Proxies will also be developed linking these satellite ocean color observations of plumes with relevant ecological (e.g., toxicity and bacteria) parameters in order to provide synoptic risk assessment maps for the San Pedro Shelf and other regions within the Southern California Bight. In this context, additional insights will be gained by characterizing the variable impact watershed type, e.g., agricultural, urban, and mixed use, has on runoff properties. Finally, effective coastal water quality management in this (and other) regions ultimately requires near real-time integration of multi-sensor, high resolution satellite data, coincident ground-based and in situ measurements, and data assimilation methods for accurate nowcasting and forecasting of the transport of stormwater runoff.

Acknowledgements

The authors would like to thank the SeaWiFS Project (Code 970.2) and the Distributed Active Archive Center (Code 902) at the Goddard Space Flight Center for the production and distribution of the SeaWiFS data, respectively. These activities are sponsored by NASA's Mission to Planet Earth Program. We also thank the NOAA National Data Center Climate Data Online (NNDC/CDO) for the raingauge-measured precipitation data. We thank Steven Weisberg, Eric Stein, Alexander Shchepetkin, Mike Mengel, and George Robertson for critical discussion of the results. The JPL effort was supported by the National Aeronautics and Space Administration through a contract with the Jet Propulsion Laboratory, California Institute of Technology.

References

Acker, J.G., Shen, S., Leptoukh, G., Serafino, G., Feldman, G., McClain, C., 2002. SeaWiFS ocean color data archive and distribution system: assessment of system performance. IEEE Transactions on Geoscience and Remote Sensing 40, 90–103.

Ackerman, D., Schiff, K., 2003. Modeling storm water mass emissions to the Southern California Bight. Journal of Environmental Engineering 129, 308–317.

Ackerman, D., Weisberg, S.B., 2003. Relationship between rainfall and beach bacterial concentrations on Santa Monica Bay beaches. Journal of Water and Health 1, 85–89.

Ackerman, D., Schiff, K.C., Weisberg, S.B., 2005. Evaluating HSPF in an arid, urbanized watershed. Journal of American Water Resources Association 41, 477–486.

Arnold, C.L., Gibbons, C.J., 1996. Impervious surface coverage: the emergence of a key environmental indicator. Journal of the American Planning Association 62, 243–258.

Bay, S., Jones, B.H., Schiff, K., Washburn, L., 2003. Water quality impacts of stormwater discharges to Santa Monica Bay. Marine Environmental Research 56, 205–223.

Beighley, R.E., Melack, J.M., Dunne, T., 2003. Impacts of California's climatic regimes and coastal land use change on streamflow characteristics. Journal of the American Water Resources Association 39, 1419–1433.

Boehm, A.B., Sanders, B.F., Winant, C.D., 2002a. Cross-shelf transport at Huntington Beach. Implications for the fate of sewage discharged through an offshore ocean outfall. Environmental Science & Technology 36, 1899–1906.

Boehm, A.B., Grant, S.B., Kim, J.H., Mowbray, S.L., McGee, C.D., Clark, C.D., Foley, D.M., Wellman, D.E., 2002b. Decadal and shorter period variability of surf zone water quality at Huntington Beach, California. Environmental Science & Technology 36, 3885–3892.

Boehm, A.B., Lluch-Cota, D.B., Davis, K.A., Winant, C.D., Monismith, S.G., 2004. Covariation of coastal temperature and microbial pollution at interannual to tidal periods. Geophysical Research Letters 31, L06309.

Bray, N.A., Keyes, A., Morawitz, W.M.L., 1999. The California Current system in the Southern California Bight and the Santa Barbara Channel. Journal of Geophysical Research 104, 7695–7714.

Burkov, V.A., Pavlova, Y.V., 1980. Description of the eddy field of the California Current. Oceanology. (English Translation) 20, 272–278.

Chao, S.-Y., 1998. Hyperpycnal and buoyant plumes from a sediment-laden river. Journal of Geophysical Research 103, 3067–3081.

Chao, S.-Y., Boicourt, W.C., 1986. Onset of estuarine plumes. Journal of Physical Oceanography 16, 2137–2149.

DiGiacomo, P.M., Holt, B., 2001. Satellite observations of small coastal ocean eddies in the Southern California Bight. Journal of Geophysical Research 106, 22521–22543.

DiGiacomo, P.M., Hamner, W.M., Hamner, P.P., Caldeira, R.M.A., 2002. Phalaropes feeding at a coastal front in Santa Monica Bay, California. Journal of Marine Systems 37, 199–212.

DiGiacomo, P.M., Washburn, L., Holt, B., Jones, B., 2004. Coastal pollution hazards in southern California observed by SAR imagery: stormwater plumes, wastewater plumes, and natural hydrocarbon seeps. Marine Pollution Bulletin 49, 1013–1024.

Dorman, C.E., Palmer, D.P., 1981. Southern California summer coastal upwelling. In: Richards, F.A. (Ed.), Coastal Upwelling. American Geophysical Union, Washington, D.C., pp. 44–56.

Fong, D.A., Geyer, W.R., 2001. Response of a river plume during an upwelling favorable wind event. Journal of Geophysical Research 106, 1067–1084.

Garvine, R.W., 1982. A steady state model for buoyant surface plume hydrodynamics in coastal waters. Tellus 34, 293–306.

Garvine, R.W., 1987. Estuary plumes and fronts in shelf waters: a layer model. Journal of Physical Oceanography 17, 1877–1896.

Geyer, W.R., Hill, P., Milligan, T., Traykovski, P., 2000. The structure of the Eel River plume during floods. Continental Shelf Research 20, 2067–2093.

Gumprecht, B., 1999. The Los Angeles River. Its Life, Death, and Possible Rebirth. The Johns Hopkins University Press, Baltimore 372 pp.

Hickey, B.M., 1979. The California Current system: hypotheses and facts. Progress in Oceanography 8, 191–279.

Hickey, B.M., 1992. Circulation over the Santa Monica-San Pedro basin and shelf. Progress in Oceanography 30, 37–115.

Hickey, B.M., 1993. Physical oceanography. In: Dailey, M.D., Reish, D.J., Anderson, J.W. (Eds.), Ecology of the Southern California Bight. University of California Press, Berkeley, pp. 19–70.

Hickey, B.M., Dobbins, E.L., Allen, S.E., 2003. Local and remote forcing of currents and temperature in the central Southern California Bight. Journal of Geophysical Research 108, 3081.

Lagerloef, G.S.E., 2000. Recent progress toward satellite measurements of the global sea surface salinity field. In: Halpern, D. (Ed.), Satellites, Oceanography and Society. Elsevier, Amsterdam, pp. 309–319.

Lahet, F., Ouillon, S., Forget, P., 2001. Colour classification of coastal waters of the Ebro river plume from spectral reflectances. International Journal of Remote Sensing 22, 1639–1664.

Lira, J., Morales, A., Zamora, F., 1997. Study of sediment distribution in the area of the Panuco river plume by means of remote sensing. International Journal of Remote Sensing 18, 171–182.

List, E.J., Gartrell, G., Winant, C.D., 1990. Diffusion and dispersion in coastal waters. Journal of Hydraulic Engineering 116, 1158–1179.

Loisel, H., Bosc, E., Stramski, D., Oubelkheir, K., Deschamps, P.-Y., 2001. Seasonal variability of the backscattering coefficient in the Mediterranean Sea based on satellite SeaWiFS imagery. Geophysical Research Letters 28, 4203–4206.

Lynn, R.J., Simpson, J.J., 1987. The California Current System: the seasonal variability of its physical characteristics. Journal of Geophysical Research 92, 12947–12966.

Mallin, M.A., Williams, K.E., Esham, E.C., Lowe, R.P., 2000. Effect of human development on bacteriological water

quality in coastal watersheds. Ecological Applications 10, 1047–1056.

Mertes, L.A.K., Warrick, J.A., 2001. Measuring flood output from 110 coastal watersheds in California with field measurements and SeaWiFS. Geology 29, 659–662.

Mertes, L.A.K., Hickman, M., Waltenberger, B., Bortman, A.L., Inlander, E., McKenzie, C., Dvorsky, J., 1998. Synoptic views of sediment plumes and coastal geography of the Santa Barbara Channel, California. Hydrological Processes 12, 967–979.

Monahan, E.C., Pybus, M.J., 1978. Colour, UV absorbance and salinity of the surface waters off the west coast of Ireland. Nature 274, 782–784.

MWD, 2002. Report on Metropolitan's Water Supplies. Metropolitan Water District of Southern California. Los Angeles, CA, 18pp.

O'Donnell, J., 1990. The formation and fate of a river plume: a numerical model. Journal of Physical Oceanography 20, 551–569.

Otero, M.P., Siegel, D.A., Fields, E.A., 2001. Satellite view of plumes and blooms in the Santa Barbara Channel; validation and description. WWW Page, http://www.icess.ucsb.edu/PnB/projects/motero2001/ASLO_2001_Poster.html.

Pineda, J., 1995. An internal tidal bore regime at nearshore stations along western USA: predictable upwelling within the lunar cycle. Continental Shelf Research 15, 1023–1041.

Pringle, J.M., Riser, K., 2003. Remotely forced nearshore upwelling in Southern California. Journal of Geophysical Research 108, 3131.

Pritchard, M., Huntley, D.A., 2002. Instability and mixing in a small estuarine plume front. Estuarine, Coastal and Shelf Science 55, 275–285.

Reeves, R.L., Grant, S.B., Mrse, R.D., Copil Oancea, C.M., Sanders, B.F., Boehm, A.B., 2004. Scaling and management of fecal indicator bacteria in runoff from a coastal urban watershed in southern California. Environmental Science & Technology 38, 2637–2648.

Sathyendranath, S. (Ed.), 2000. Remote Sensing of Ocean Colour in Coastal and Other Optically-Complex Waters, vol. 3. IOCCG, Dartmouth, Canada, 140pp.

Schiff, K.C., Bay, S., 2003. Impacts of stormwater discharges on the nearshore benthic environment of Santa Monica Bay. Marine Environmental Research 56, 225–243.

Schiff, K.C., Allen, M.J., Zeng, E.Y., Bay, S.M., 2000. Southern California. Marine Pollution Bulletin 41, 76–93.

Siddorn, J.R., Bowers, D.G., Hoguane, A.M., 2001. Detecting the Zambezi River plume using observed optical properties. Marine Pollution Bulletin 42, 942–950.

Stumpf, R.P., Gelfenbaum, G., Pennock, J.R., 1993. Wind and tidal forcing of a buoyant plume, Mobile Bay, Alabama. Continental Shelf Research 13, 1281–1301.

Svejkovsky, J., Jones, B., 2001. Satellite imagery detects coastal stormwater and seawage runoff. EOS 82, 621–630.

Sverdrup, H.U., Fleming, R.H., 1941. The waters off the coast of southern California, March to July 1937. Bulletin of the Scripps Institution of Oceanography 4, 261–378.

Toole, D.A., Siegel, D.A., 2001. Modes and mechanisms of ocean color variability in the Santa Barbara Channel. Journal of Geophysical Research 106, 26985–27000.

Turhollow, A.F., 1975. A history of the Los Angeles District, US Army Corps of Engineers, 1989-1965. US Army Engineer District, Los Angeles, 440pp.

Vasilkov, A.P., Burenkov, V.I., Ruddick, K.G., 1999. The spectral reflectance and transparency of river plume waters. International Journal of Remote Sensing 20, 2497–2508.

Vaze, J., Chiew, F.H.S., 2003. Study of pollutant washoff from small impervious experimental plots. Water Environment Research 39, 1160–1169.

Warrick, J.A., Mertes, L.A.K., Washburn, L., Siegel, D.A., 2004. Dispersal forcing of southern California river plumes, based on field and remote sensing observations. Geo-Marine Letters 24, 46–52.

Washburn, L., McClure, K.A., Jones, B.H., Bay, S.M., 2003. Spatial scales and evolution of stormwater plumes in Santa Monica Bay. Marine Environmental Research 56, 103–125.

Winant, C.D., Bratkovich, A.W., 1981. Temperature and currents on the southern California shelf: a description of the variability. Journal of Physical Oceanography 11, 71–86.

Yankovsky, A.E., Hickey, B.M., Munchow, A.K., 2001. Impact of variable inflow on the dynamics of a coastal buoyant plume. Journal of Geophysical Research 106, 19809–19824.